

1 **Quantification of long-term doxorubicin response dynamics in breast cancer**  
2 **cell lines to direct treatment schedules**

3  
4 Grant Howard<sup>1</sup>, Tyler A. Jost<sup>1</sup>, Thomas E. Yankeelov<sup>1, 3-7</sup>, Amy Brock <sup>\*1,2</sup>

5 Departments of <sup>1</sup>Biomedical Engineering, <sup>2</sup>Cell and Molecular Biology, <sup>3</sup>Diagnostic Medicine,  
6 and <sup>4</sup>Oncology, The University of Texas at Austin, Austin TX;

7 <sup>5</sup>Oden Institute for Computational Engineering and Sciences, The University of Texas at Austin,  
8 Austin, TX;

9 <sup>6</sup>Livestrong Cancer Institutes, The University of Texas at Austin, Austin, TX;

10  
11 <sup>7</sup>Department of Imaging Physics  
12 The University of Texas MD Anderson Cancer Center  
13 Houston, TX  
14  
15  
16

17 \* Corresponding author

18 Email: amy.brock@utexas.edu  
19  
20

## 1 **Abstract**

2           While acquired chemoresistance is recognized as a key challenge to treating many types of  
3 cancer, the dynamics with which drug sensitivity changes after exposure are poorly characterized.  
4 Most chemotherapeutic regimens call for repeated dosing at regular intervals, and if drug  
5 sensitivity changes on a similar time scale then the treatment interval could be optimized to  
6 improve treatment performance. Theoretical work suggests that such optimal schedules exist, but  
7 experimental confirmation has been obstructed by the difficulty of deconvolving the simultaneous  
8 processes of death, adaptation, and regrowth taking place in cancer cell populations. Here we  
9 present work characterizing dynamic changes in sensitivity to the chemotherapeutic doxorubicin  
10 in three breast cancer cell lines subjected to treatment schedules varying in concentration, interval  
11 between pulse treatments, and number of sequential pulse treatments. Cell populations are  
12 monitored longitudinally through automated imaging for 600-800 hours, and this data is used to  
13 calibrate a family of cancer growth models derived from the bi-exponential model which  
14 characterizes resistant and sensitive subpopulations. We identify a model incorporating both a  
15 period of growth arrest in surviving cells and a delay in the death of chemosensitive cells which  
16 outperforms the original bi-exponential growth model in Akaike Information Criterion based  
17 model selection, and use the calibrated model to quantify the performance of each drug schedule.  
18 We find that the inter-treatment interval is a key variable in determining the performance of  
19 sequential dosing schedules and identify an optimal retreatment time for each cell line which  
20 extends regrowth time by 40%-106%, demonstrating that the time scale of changes in  
21 chemosensitivity following doxorubicin exposure allows optimization of drug scheduling by  
22 varying this inter-treatment interval.

23 **Key words:** chemoresistance, chemotherapy, proliferation, mathematical modeling, treatment  
24 scheduling

## 1 **Introduction**

2 Cancer is the second most prevalent cause of death in the United States, and acquired  
3 chemoresistance is a common cause of treatment failure in cancer(1,2). While many studies have  
4 investigated the biochemical mechanisms of chemoresistance, predicting the onset of resistance  
5 and the population dynamics of sensitive and resistant cells remains a challenge(3–6).

6 Early chemotherapy treatment schedules, based on the approach of maximally-tolerated  
7 dose to achieve maximal killing of tumor cells, assumed a homogenous, exponentially growing  
8 cell population(7,8). Subsequent studies have pointed to the significance of intratumor  
9 heterogeneity in cell growth rate and drug sensitivity(9–18). Norton and others established that  
10 tumor kill is proportional to growth rate(19–21), and adjuvant chemotherapy schedules for breast  
11 cancer were revised to decrease the interval of therapy for fast-growing TNBC(22–24). Other  
12 studies point to metronomic therapy and adaptive therapy as potential improvements for breast  
13 cancer scheduling(25–29).

14 Mathematical modeling of drug responses has developed optimal solutions for drug dosing  
15 under a variety of model assumptions(30–33), highlighting the opportunity to improve cancer  
16 treatment by optimizing drug schedules. However, these efforts have generally been purely  
17 theoretical. Under the necessarily simplified assumptions of these drug sensitivity models, it is  
18 possible to find a true mathematical optimum, but these studies have not explored the magnitude  
19 or form of deviation between their models and experimental observations. This reveals a need for  
20 methods to experimentally test the response to drug schedules, and to use those experimental  
21 results to inform and calibrate models of drug response in cancer. Robust predictive models of  
22 drug response are a necessary step towards the ultimate goal of patient-specific predictive models  
23 of therapy-response and relapse.

24 A challenge in modeling chemoresistance is that the state of drug sensitivity is often  
25 represented as binary – sensitive or resistant. Clinically, resistance is usually inferred at very  
26 coarse time intervals – a patient is retrospectively assessed as sensitive or resistant to a course of

1 treatment as a whole. In *in vitro* work, cell lines are labeled as sensitive or resistant as well, based  
2 on their stable drug sensitivity(34,35). This approach may obscure key underlying characteristics  
3 of the system if drug sensitivity is heterogeneous in the cancer cell population. In addition, cells  
4 may change drug sensitivity over time or in response to environmental conditions, adding temporal  
5 heterogeneity(36–41) . The consequence is that cells display a distribution of responses to drug  
6 exposure and this distribution may vary with time(42–50). Experimental work describing the  
7 distribution of drug sensitivity in cancer cell populations, and the temporal changes arising from  
8 cell plasticity, is key to understanding drug resistance at the population level.

9 In this work, we seek to quantify the dynamic changes in drug sensitivity following  
10 treatment to iteratively optimize treatment schedules in a series of *in vitro* experiments subjecting  
11 three breast cancer cell lines to a series of pulsed drug perturbations which vary in drug  
12 concentration, inter-treatment interval, and number of serial drug exposures. Long-term  
13 automated time-lapse microscopy enables quantitation of population dynamics in multiple  
14 replicates, doses and regimens over days to weeks. Here we measured up to 12 individual culture  
15 wells in 3 cell types treated with a range of 9 doses and 13 regimens.

16 By calibrating the resulting data to a mathematical model, we quantify the distribution of  
17 the underlying populations with respect to model parameters of interest including resistant fraction,  
18 relapse growth rate, and sensitive cell death rate. Additionally, we characterize the dynamics of  
19 both the relapse and dying populations. In this study, we sought to capture the fact that sensitive  
20 cells do not respond to drug treatment by immediately undergoing cell death and resistant cells do  
21 not respond by continuing to proliferate at the same rate as untreated cells. Rather, the processes  
22 of cell death, cell cycle arrest, and cell growth after treatment are complex and these time scales  
23 may overlap—with some cells continuing to die in response to drug treatment, while others are  
24 simultaneously recovering from a period of arrest and beginning to proliferate.

25 Model selection is used to identify three phenomenological models, from a family of 18  
26 related models which vary in the dynamics defining cell growth and death in treated populations,  
27 which most accurately parameterize the data. Time-lapse microscopy data is used to calibrate the

1 three phenomenological models, and select the model which best characterizes the data. The  
2 optimal model is then used to quantify the impact of the tested drug schedules on cancer cell  
3 population, and identify schedules with superior performance. This demonstrates a method for  
4 optimizing drug schedules using mathematical models of drug sensitivity which are experimentally  
5 calibrated using high throughput in-vitro experiments. This method could be extended to  
6 additional drugs, drug combinations, and cancer types.

7

## 8 **Model description**

9 We used a simple mathematical model that treats cancer cell population dynamics as a  
10 process consisting of a decreasing drug-sensitive subpopulation of tumor cells, and an  
11 independently growing drug-resistant subpopulation. This model has successfully described tumor  
12 dynamics in non-small cell lung cancer, melanoma(51), multiple myeloma(52), and ovarian  
13 cancer(53). After exposure to drug, the net fitness of the drug-sensitive ( $S$ ) cells is represented in  
14 terms of an exponential decay or “tumor cell kill” rate  $k$ , and the net fitness of the resistant ( $R$ )  
15 cancer cells as an exponential growth rate  $g_r > 0$ , and the initial fraction of drug-resistant cells by  
16  $0 \leq f_r \leq 1$ . Additionally, the resistant cancer cells may experience a period of proliferation arrest  
17  $t_r \geq 0$ . (The  $R$  and  $S$  designations are solely with respect to the specific drug exposure being  
18 examined, and are not intended to specify any particular mechanism of action.) To analyze the  
19 response of a population of  $S$  and  $R$  cells to drug treatment, we use a system of two ordinary  
20 differential equations (1 and 2) coupled by the total cell number (equation 3) to describe the  
21 dynamics of the  $S$  and  $R$  subpopulations.

$$\frac{dR}{dt} = g_r R \left(1 - \frac{N}{N_{max}}\right) H(t - t_r) \quad (1)$$

$$\frac{dS}{dt} = -kS \quad (2)$$

$$N = R + S \quad (3)$$

1 Initial conditions are specified using the resistant fraction,  $f_r$ , in equations 4 and 5.  $H(x)$  is  
 2 the Heaviside step function, which is 0 for negative values of the argument and 1 for positive  
 3 values of the argument.

$$R(t_0) = f_r N_0 \quad (4)$$

$$S(t_0) = (1 - f_r) N_0 \quad (5)$$

4 To better understand how growth and death dynamics impact drug sensitivity of the overall  
 5 cell population, we use automated image analysis of time lapse microscopy data to calibrate three  
 6 families of phenomenological models of the population-level drug response. Resistant cells  
 7 experience a period of growth arrest,  $t_r$ , followed by logistic growth at rate,  $g_r$ . Sensitive cells die  
 8 at rate  $k$ , which is subject to variation in the doxorubicin response(54), and three models for  $k$  are  
 9 considered: 1) a time-delayed model of  $k$ , such that the value varies between cell growth at the  
 10 initial growth rate of  $g_0$  and cell death at a maximum rate of  $k_d$  with exponential decay from  $g_0$  to  
 11  $k_d$  at a time constant of  $t_d$  (equation 6), 2) a time-delayed model of  $k$  such that the value varies  
 12 linearly between cell growth at the initial growth rate of  $g_0$  and cell death at a maximum rate of  $k_d$   
 13 over a total time of  $t_d$  (equation 7), 3) a constant value of  $k$  (equation 8). Models 1 and 2 each  
 14 include 6 total parameters, while the simpler model 3 includes 5.

15

$$k = k_d - (g_0 + k_d) \exp\left(-\frac{t}{t_d}\right) \quad (6)$$

$$k = k_d - (g_0 + k_d) \left(1 - \frac{t}{t_d}\right) H(t_d - t) \quad (7)$$

$$k = k_d \quad (8)$$

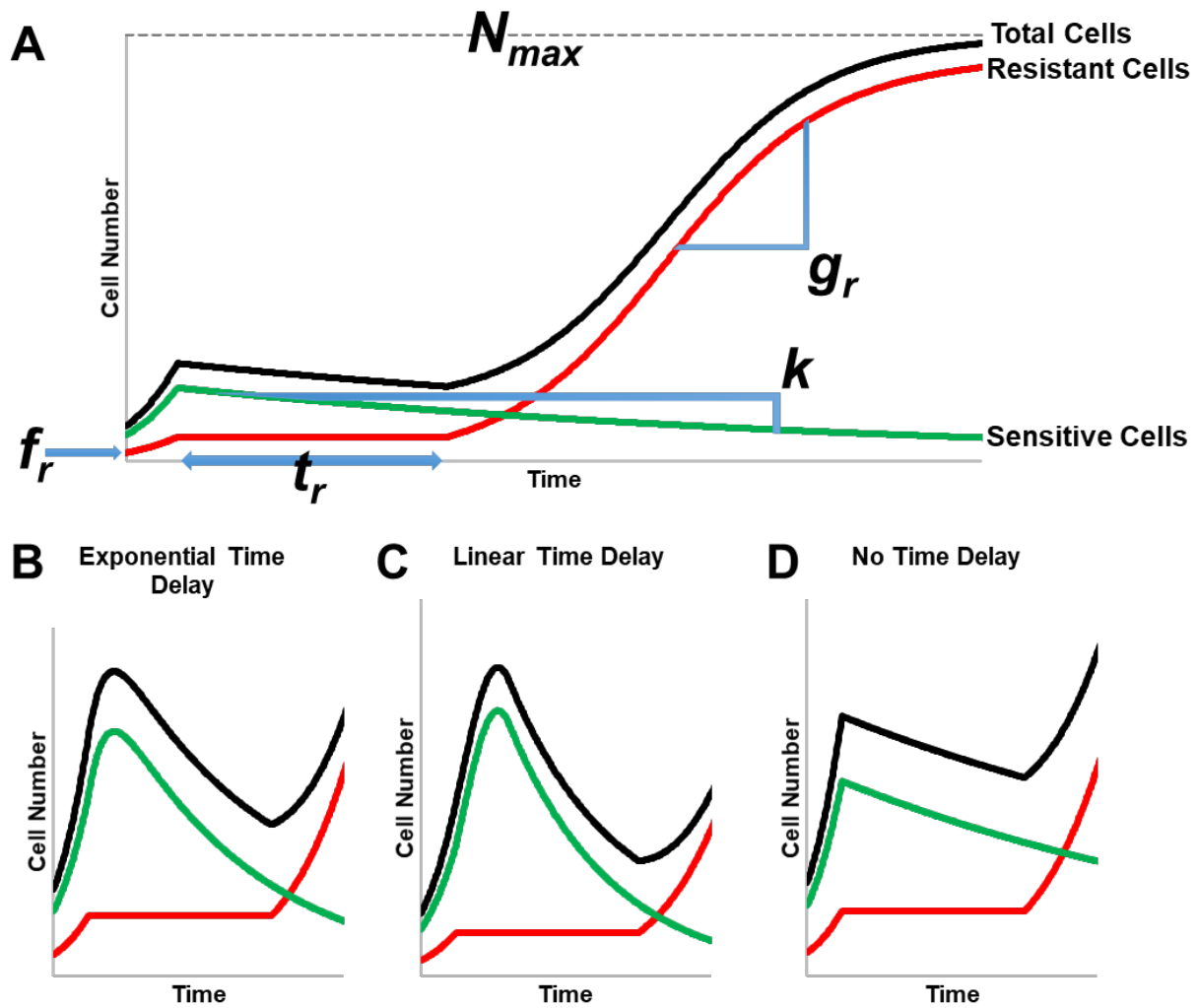
16

Symbol	Model Parameter Description	Parameter Assignment
$f_r$	Resistant fraction	Calibrated
$g_r$	Relapse growth rate	Calibrated
$t_r$	Proliferation delay	Measured via clustering analysis
$k_d$	Sensitive cell death rate	Calibrated

$t_d$	Time constant for death delay	Calibrated
$g_0$	Pre-treatment growth rate	Calibrated
$N_{max}$	Carrying capacity	Calibrated

1 **Table 1. Summary of model parameters**

2 Model 1 represents a case in which cells stochastically transition from proliferating to  
3 dying. At the time of treatment, the cell population is still proliferating (represented in the model  
4 as a negative net death rate for this cell compartment). The net death rate smoothly transitions from  
5 proliferation to death and approaches the maximum value of  $k_d$  exponentially at a time constant of  
6  $t_d$ . Model 2 represents a case where cells take time,  $t_d$ , to halt proliferation, again transitioning  
7 from initially proliferating at a rate of  $g_0$  at the time drug exposure begins, to an eventual maximum  
8 death rate of  $k_d$ . Model 3 represents the simplest case with the minimum number of parameters;  
9 here the population responds to drug exposure rapidly enough on the time scale of the experiment  
10 for transition time to be negligible. These are nested models, and we will evaluate the need for the  
11 additional parameters, which increase the complexity of the models, using model selection criteria  
12 when fitting the data to the models.  
13



1

2 **Fig 1. Model structures** illustrated with curves for total cell number (black) partitioned into  
3 resistant (red) and sensitive (green) fractions. Regions of the curves are marked to show the  
4 effects of key model parameters (A). The effects of three different models of  $k$  are shown for  
5 model 1 with an exponential time delay on  $k$  (B), model 2 with a linear time delay on  $k$  (C) or  
6 model 3 with no time delay on  $k$  (D).

7



## 1 **Model identifiability**

2           To test the ability of our modeling framework to accurately extract parameter values and  
3 select among models, each model within the family described above was used to calibrate  
4 simulated data. This model family includes three sets of assumptions concerning the form of  $k$ ,  
5 which are described as models 1, 2, and 3; independently,  $t_r$  can be zero or non-zero. Six simulated  
6 data sets, labeled A through F and each containing 1000 time series of cell number, were generated  
7 from these six sets of assumptions concerning the underlying ground truth. For each data set,  
8 parameter values were randomly generated from within a physiologically reasonable parameter  
9 space (details provided in **Supporting Information, model identifiability results**), a cell number  
10 vector was generated based on those parameter values, and Gaussian random noise was added to  
11 each data point of the cell number vector to simulate measurement error. We were interested in  
12 determining whether the underlying model could be identified from the cell number data alone, or  
13 whether the  $t_r$  value must also be specified to obtain accurate parameter values. Additionally, we  
14 sought to determine whether it was possible to reduce the number of free parameters by fixing  
15  $N_{max}$ . This resulted in a total of 18 models:  $k$  selected from models 1, 2, or 3,  $t_r$  calibrated, assumed  
16 to be 0, or given as input, and  $N_{max}$  either calibrated or fixed. Each data set was used to calibrate  
17 the 18 models, summarized in **Table 2**.

Model	Assignment of $t_r$ , proliferation delay in $R$ cells	$k$ , death delay in $S$ cells	$N_{max}$	PCC
1	known and given as input	Exponential	Calibrated	0.99
2	known and given as input	Linear	Calibrated	0.99
3	known and given as input	None	Calibrated	0.99
4	calibrated	Exponential	Calibrated	0.34
5	calibrated	Linear	Calibrated	0.28
6	calibrated	None	Calibrated	0.25
7	0	Exponential	Calibrated	0.93
8	0	Linear	Calibrated	0.94
9	0	None	Calibrated	0.99
10	known and given as input	Exponential	Fixed	0.74
11	known and given as input	Linear	Fixed	0.72
12	known and given as input	None	Fixed	0.71
13	calibrated	Exponential	Fixed	0.27
14	calibrated	Linear	Fixed	0.27
15	calibrated	None	Fixed	0.24
16	0	Exponential	Fixed	0.23
17	0	Linear	Fixed	0.29
18	0	None	Fixed	0.68

1 **Table 2. Summary of model assumptions.** Pearson's correlation coefficient (PCC)  $f_r$  for each  
2 model calibrated with data generated based on a matching ground truth for  $t_r$  and the form of  $k$ .

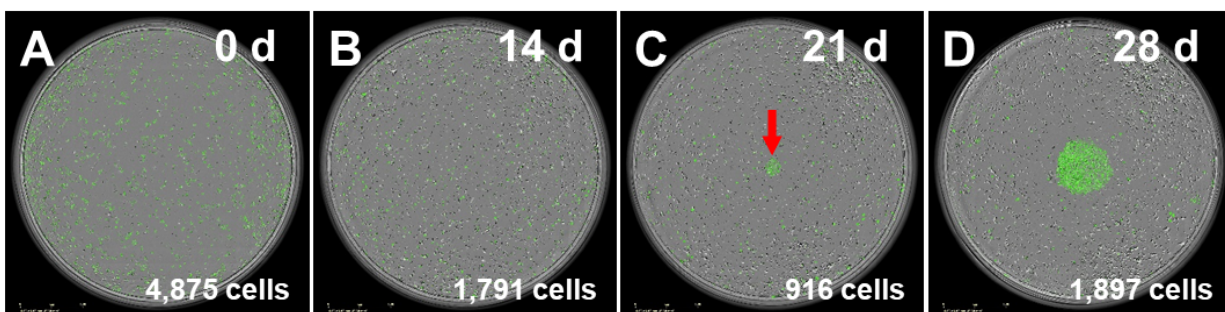
3

4 To check the ability of each model to extract accurate parameter values from the simulated  
5 data sets, Pearson's correlation coefficients (PCC) between the known and calibrated values for  
6 the model parameters were computed for each combination of model and simulated data set (**Table**  
7 **S3**). Comparing PCC values for each model 1 through 9 to its matching model 10 through 18  
8 reveals that calibration of the carrying capacity is necessary. Use of a fixed value for carrying

1 capacity significantly reduces the ability of the modeling framework to accurately identify  
2 parameter values (see **Fig S3**). Consequently, models 10 through 18 were excluded from further  
3 analysis

4 The model sets 1, 4 and 7; 2, 5, and 8; and 3, 6, and 9 each vary solely in the handling of  
5  $t_r$ , the period of growth arrest after drug exposure. Models 4, 5, and 6 extracted parameter values  
6 with a PCC of 0.34 or less even when matched to data sets generated from matching model  
7 assumptions, while models 1, 2, and 3 each extract parameter values with a PCC of 0.99. Closer  
8 consideration revealed that the  $t_r$  and  $f_r$  values are not uniquely identifiable in data with any amount  
9 of noise (see **Fig S2**). Based on this difference in accuracy, models 4, 5, and 6 were excluded from  
10 further analysis. Models 7, 8, and 9, in which  $t_r = 0$ , extract parameter values with PCC 0.93 or  
11 greater from data sets D-F, generated from matching model assumptions, but with PCC of 0.20 or  
12 less when calibrated to data sets A-C generated with  $t_r \neq 0$  (**Table S3**). The key question, which  
13 must be resolved experimentally, is whether  $t_r$  is in fact non-zero, as computational work alone  
14 proved unable to determine this in the analysis stage. Examination of the raw data demonstrated  
15 that the period of proliferation arrest,  $t_r$ , can be non-zero, and in some cases is substantial (**Fig 2**).  
16 Consequently, models 7-9 were removed from consideration, with models 1-3 included for future  
17 analysis.

18



20 **Fig 2. Micrograph example illustrating doxorubicin induced proliferation delay**

21 In this example demonstrating a doxorubicin induced proliferation delay, after exposure to 150  
22 nM doxorubicin at time 0 (A) MCF7 cells stop proliferating and remain in arrest for 315 hours.  
23 At 14 days (B), cells have died off in the intervening time, and proliferation has not occurred,

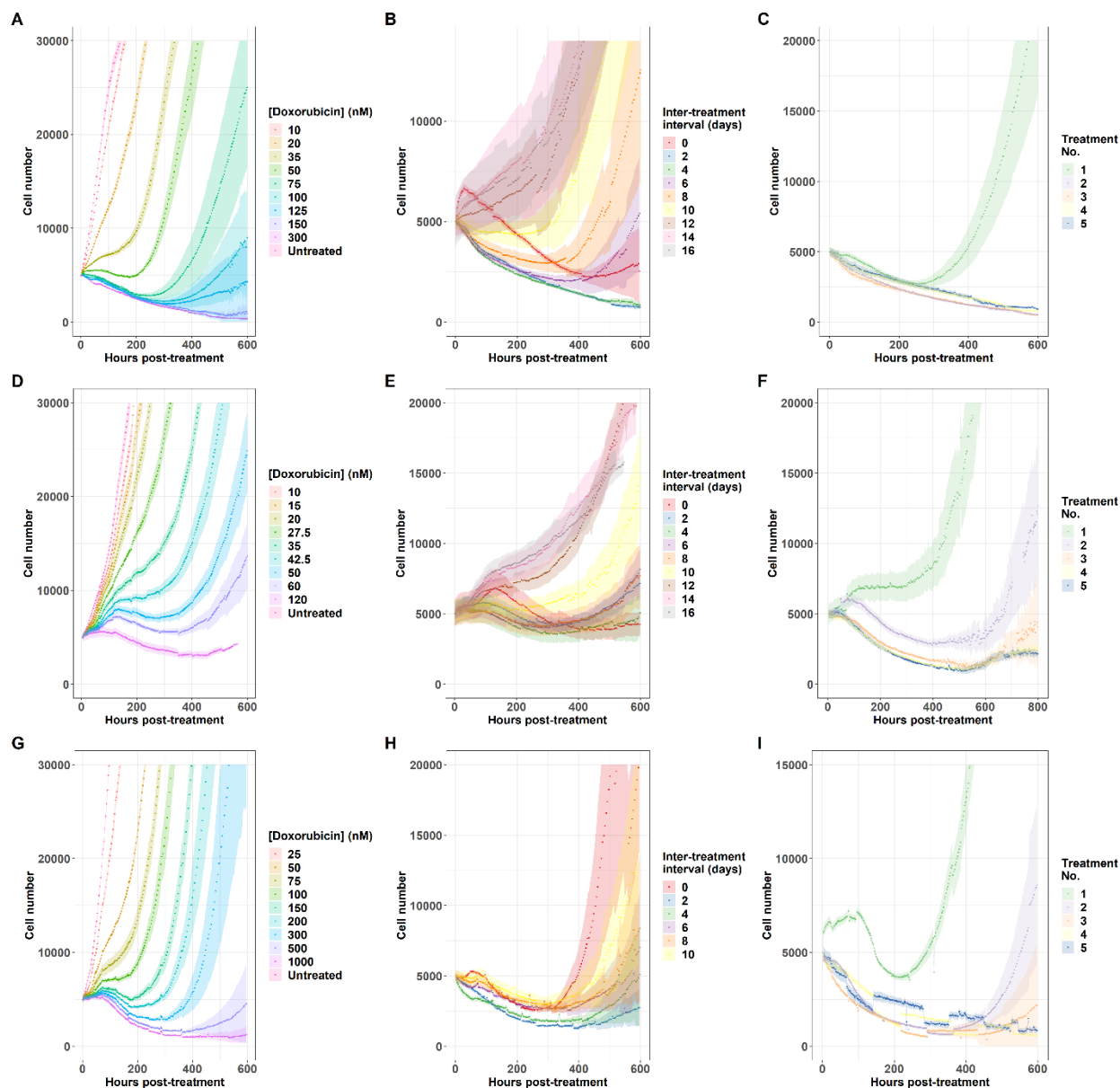
1 and at 21 days (C), proliferation has produced a small patch of cells indicated by the red arrow;  
2 proliferation then continues and produces a patch of hundreds of cells by 28 days (D). Untreated  
3 cells grow to confluence in approximately four days.  
4

5 The Akaike information criterion (AIC) was applied to the calibrations generated by  
6 models 1-3 on simulated data sets A-F to test its ability to identify the underlying model structure  
7 in cases where the ground truth is known independently. When the AIC is computed for three  
8 otherwise equivalent models which vary in the form of  $k$ , it selects the model which matches the  
9 ground truth of the simulated data in 97% of cases where there is no death delay, in 87% of cases  
10 if the death delay has an exponential form, and in 84% of cases when the death delay has a linear  
11 form. In each case, the correct model is identified in a majority of simulated data sets,  
12 demonstrating the utility of the AIC at identifying the model which best matches the ground truth.

## 13 **RESULTS**

### 14 **Quantification of long term population level response**

15 To determine the dynamics of the long-term cell population response to doxorubicin, breast  
16 cancer cell populations were subjected to one to five sequential doxorubicin exposures, with the  
17 drug concentration, interval between drug exposures, or number of drug exposures allowed to vary.  
18 Time lapse microscopy and automated image analysis was used to quantify the cell number  
19 throughout the treatment period and up to four weeks after the final dose.



## 2 Fig 3. Cell population response to doxorubicin regimens

3 Population level response to 24 hour doxorubicin exposures is quantified as doxorubicin  
4 concentration varies in the MCF7 cell line (A), the BT474 cell line (D), and the MDA-MB-231  
5 cell line (G), as the interval between two 24 hour doxorubicin exposures varies at 75 nM in the  
6 MCF7 cell line (B), at 35 nM in the BT474 cell line (E), and at 200 nM in the MDA-MB-231 cell  
7 line (H), and as the number of sequential 24 hour doxorubicin exposures varies at a two day interval  
8 and 75 nM in the MCF7 cell line (C), at a zero day interval (continuous exposure) and 35 nM in  
9 the BT474 cell line (F), and at a two day interval and 200 nM in the MDA-MB-231 cell line (I).  
10 Each curve represents the average of six (A, D, G) or 12 (B, C, E, F, H, I) replicate samples, and  
11 95% confidence intervals are marked by the shaded regions. All curves are aligned such that  $t =$   
12 0 is the beginning of the final drug exposure for that treatment group.

1

2       The long term response to a 24 hour doxorubicin pulse varies not only with drug  
3 concentration (**Fig 3A, 3D, 3G**), but also with the cell population's history of previous exposure,  
4 even if the total dose delivered remains constant (**Fig 3B-C, 3E-F, 3H-I**). Population behavior  
5 varies over time, and the response observed at any single time point (such as 48 or 72 hours, which  
6 are frequently chosen as endpoints for single time-point observations) does not accurately  
7 characterize the overall dynamic response. Visual assessment of these cell number curves offers  
8 some intuition on the relative strength of the drug treatments: A cell population that is sensitive  
9 to a drug treatment may manifest in a curve that dips to a deeper minimum, or takes longer to  
10 resume net population growth, or shows slower population growth over the long term. As  
11 expected, for a single administration of doxorubicin, these effects of treatment increase with dose  
12 (**Fig 3A, 3D, 3G**). When multiple doses of the same concentration are administered, the total  
13 amount of drug increases with the number of exposures; this generates the similarly intuitive result  
14 that the impact of the treatment increases when going from one treatment to two sequential  
15 treatments (**Fig 3C, 3F, 3I**).

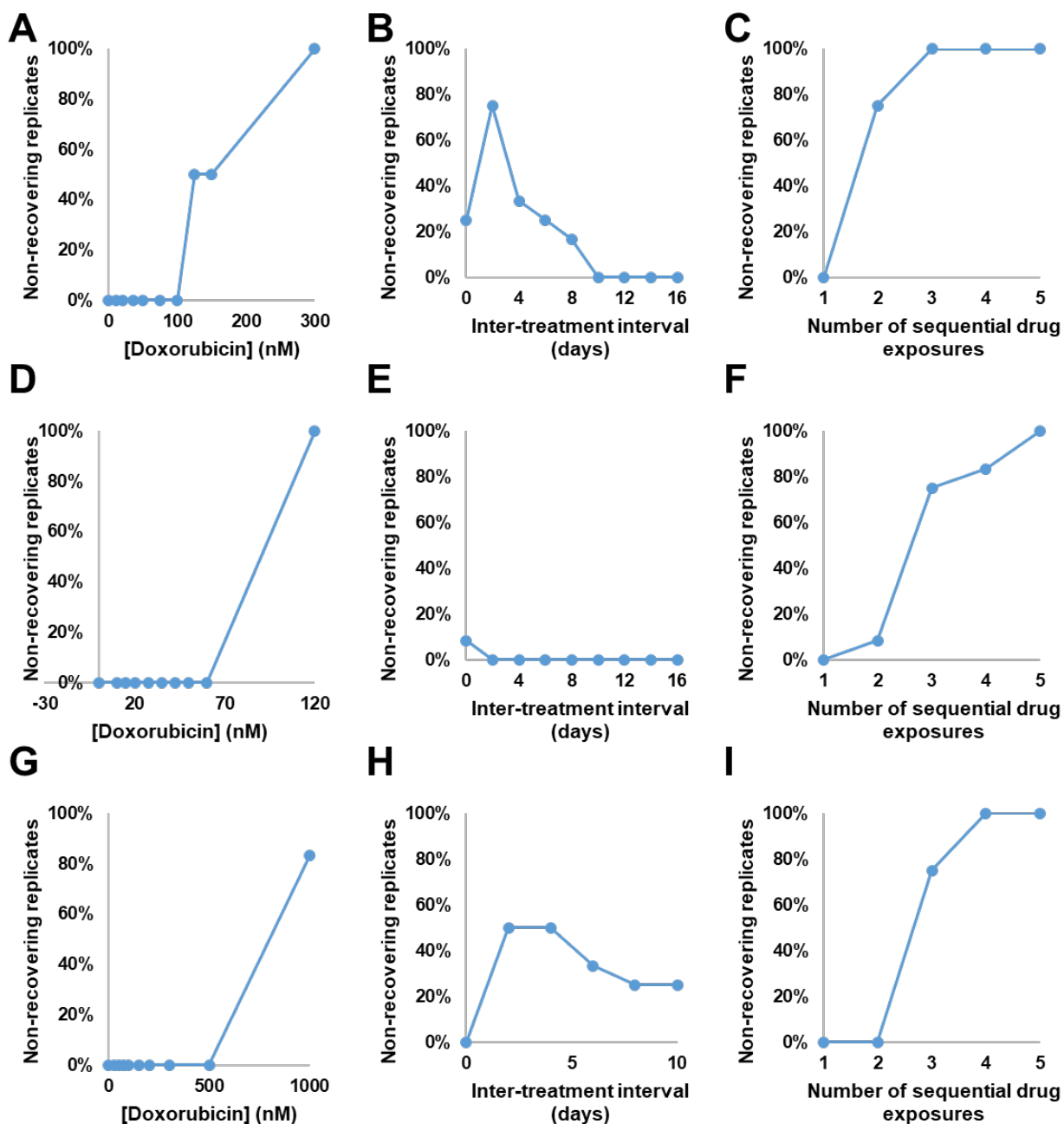
16       When the total drug exposure for each treatment group is held constant while the interval  
17 between the two exposures is varied, the cell population response curves vary considerably (**Fig**  
18 **3B, 3E, 3H**). This indicates that the drug sensitivity of all three cell lines varies dynamically, such  
19 that the timing of a second drug exposure has a profound effect on the effectiveness of the second  
20 treatment. While these observations can be made on a qualitative level from the cell number  
21 curves, calibrating these experimental results to the models discussed above allows for quantitative  
22 investigation of the variation in response.

### 23 **Fraction of non-recovering replicates**

24       Under some treatment regimens, we observe a bifurcation in the response: some replicate  
25 cultures recover proliferative capacity during the experiment, while others do not (and therefore  
26 exhibit only cell death throughout the experiment). This necessitates split handling of the analysis

1 as well, since the resistant population properties cannot be obtained in cases where no cells were  
2 resistant to the treatment. The fraction of replicate cultures which do not recover in each treatment  
3 group is shown in **Fig 4**, and these wells are excluded from the analysis of resistant cell  
4 populations.

5



6

1 **Fig 4. Fraction of non-recovering replicate cell populations.**

2 The percentage of replicate cultures which did not recover during the course of the experiment is  
3 shown as doxorubicin concentration varies in the MCF7 cell line (A), the BT474 cell line (D),  
4 and the MDA-MB-231 cell line (G), as the interval between two 24 hour doxorubicin exposures  
5 varies at 75 nM in the MCF7 cell line (B), at 35 nM in the BT474 cell line (E), and at 200 nM in  
6 the MDA-MB-231 cell line (H), and as the number of sequential 24 hour doxorubicin exposures  
7 varies at a two day interval and 75 nM in the MCF7 cell line (C), at a zero day interval  
8 (continuous exposure) and 35 nM in the BT474 cell line (F), and at a two day interval and 200  
9 nM in the MDA-MB-231 cell line (I). Each value is the percentage of 6 (A, D, G) or 12 (B, C,  
10 E, F, H, I) replicates.  
11

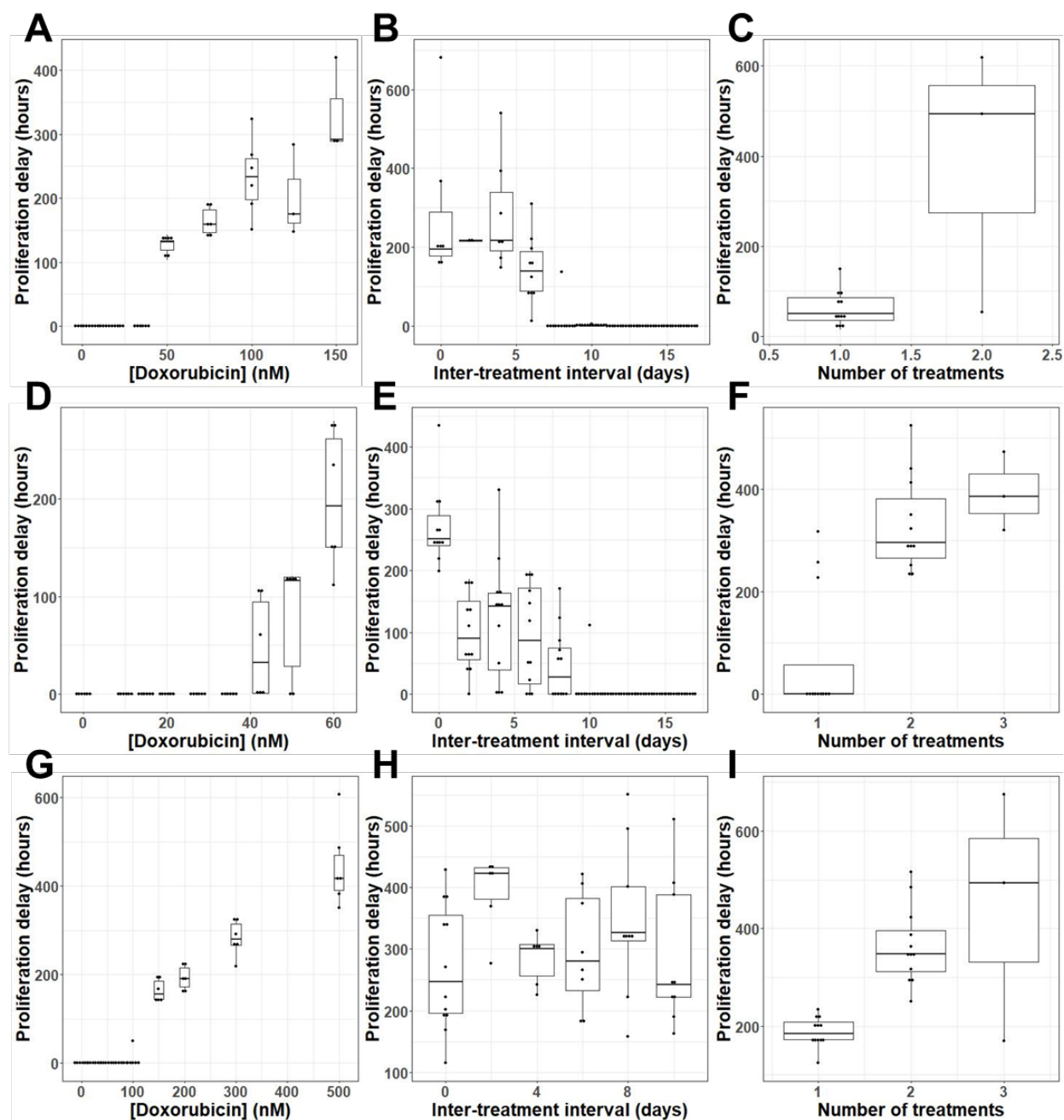
12 Although this phenomenon hinders analysis of some resistant cell properties, it also reveals  
13 which treatment regimens are capable of eliminating the entire experimental cancer cell  
14 population. The bifurcation indicates that these treatments should not be assumed to be completely  
15 effective against the cancer cell population; rather, it is sufficient for resistant cells to be rare  
16 enough in the population as a whole that the initial population of approximately 2,000 seeded cells  
17 is too low to ensure that a resistant cell will be present. Despite this caveat, these conditions do  
18 represent the practical limits of treatment regimens that can be investigated in the 96 well format.  
19 In the MCF7 cell line, doxorubicin concentrations of 125 nM or higher may result in non-  
20 recovering replicates (**Fig 4A**), and two or more sequential treatments at 75 nM may result in non-  
21 recovering replicates (**Fig 4C**). In the BT474 cell line, a doxorubicin concentration of 120 nM  
22 resulted in no recovering wells (**Fig 4D**), and two or more sequential exposures to 35 nM  
23 doxorubicin resulted in some non-recovering wells (**Fig 4F**). Similarly, in the MDA-MB-231 cell  
24 line, doxorubicin at a concentration of 1  $\mu$ M (**Fig 4G**) or three or more exposures to 200 nM  
25 doxorubicin (**Fig 4I**) may result in non-recovering replicates. While the concentration thresholds  
26 vary from cell line to cell line, in each of these cases the fraction of non-recovering wells increases  
27 with the total drug exposure within a cell line.

28 When the inter-treatment interval is varied with the total drug exposure held constant, we  
29 find that the fraction of non-recovering wells peaks in the MCF7 cell line at 75% (nine replicates  
30 out of 12) with a two day interval (**Fig 4B**), then declines to 0% at intervals of 10 or more days.  
31 In the BT474 cell line, 8% (one replicate out of 12) fails to recover in the zero interval (continuous



1 treatment) group, with all wells recovering at longer intervals (**Fig 4E**). In the MDA-MB-231 cell  
2 line, the fraction of wells which do not recover peaks at 50% (six out of 12 replicate wells) at an  
3 interval of 2 or 4 days, and declines at longer intervals (**Fig 4H**). In each cell line this again  
4 suggests that the drug sensitivity of these populations varies dynamically over this period of  
5 approximately two weeks after an initial drug exposure.

## 1 Proliferation delay, $t_r$



## 2 Fig 5. Proliferation delay, $t_r$ varies with dosing regimen

3 Length of growth arrest of resistant cells ( $t_r$ ) is displayed as a Tukey box-and-whiskers plot as  
4 doxorubicin concentration varies in the MCF7 cell line (A), the BT474 cell line (D), and the MDA-  
5 MB-231 cell line (G), as the interval between two 24 hour doxorubicin exposures varies at 75 nM  
6 in the MCF7 cell line (B), at 35 nM in the BT474 cell line (E), and at 200 nM in the MDA-MB-  
7 231 cell line (H), and as the number of sequential 24 hour doxorubicin exposures varies at a two

1 day interval and 75 nM in the MCF7 cell line (C), at a zero day interval (continuous exposure) and  
2 35 nM in the BT474 cell line (F), and at a two day interval and 200 nM in the MDA-MB-231 cell  
3 line (I). The number of replicates in each group varies between 3 and 12; all replicates in which  
4 recovery is observed are included (see Fig 4).

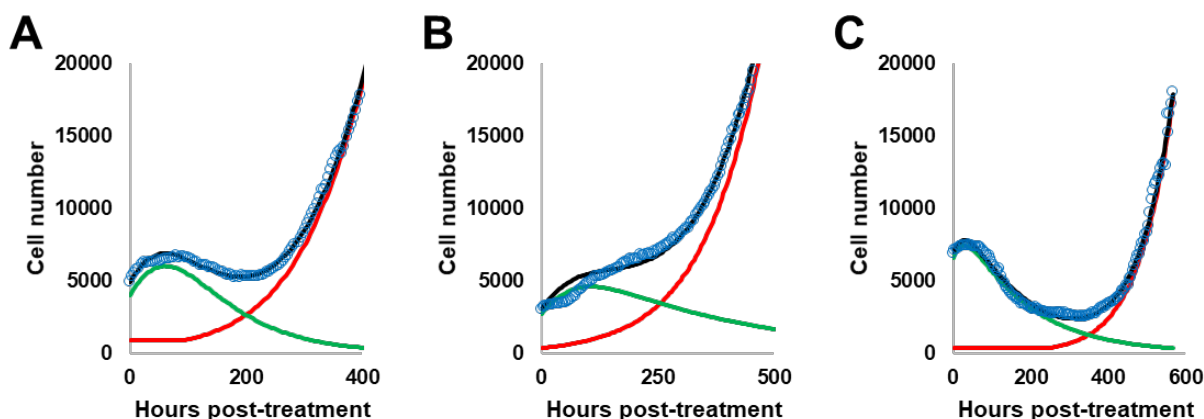
5  
6 The model identifiability analysis demonstrates that, if a period of growth arrest is present  
7 in experimental data, then it must be incorporated into the growth model to obtain accurate  
8 parameter values *via* model calibration (**Fig S2**). Growth arrest does occur under some of the  
9 treatment regimens investigated in this series of experiments. Density based clustering analysis  
10 with manual correction for common errors is used to identify the restart of proliferation in replicate  
11 cultures which experience a period of growth arrest (**Fig 5**). When the concentration of  
12 doxorubicin in a single exposure is varied, a threshold is observed with concentrations of 50 nM  
13 or higher inducing growth arrest in the MCF7 cell line (**Fig 5A**), concentrations of 42.5 nM of  
14 higher inducing growth arrest in the BT474 cell line (**Fig 5D**), and concentrations of 150 nM or  
15 higher inducing growth arrest in the MDA-MB-231 cell line (**Fig 5G**). In the MCF7 cell line,  
16 when the interval between two 75 nM doxorubicin exposures is varied, the period of growth arrest  
17 decreases as the inter-treatment interval increases (**Fig 5B**), with intervals of 0-4 days experiencing  
18 over 200 hours of growth arrest and with some replicates at intervals of 8 or more days  
19 experiencing no growth arrest at all; since an initial 75 nM exposure results in approximately 125  
20 hours of growth arrest, this suggests dynamic variation in drug sensitivity over this period of  
21 approximately two weeks. Likewise, in the BT474 cell line, as the interval between two 35 nM  
22 doxorubicin exposures is varied the period of growth arrest decreases with intervals of 10 days or  
23 longer resulting in no growth arrest (**Fig 5E**). Similarly, when the MDA-MB-231 cell line is  
24 exposed to two 200 nM drug pulses, the period of growth arrest is elevated for at least 10 days,  
25 with a peak of over 400 hours with a two day interval between exposures (**Fig 5H**). When the  
26 number of sequential drug exposures at a two day interval is varied, the period of growth arrest  
27 increases significantly after a second treatment in the MCF7 cell line (**Fig 5C**), the BT474 cell line  
28 (**Fig 5F**), and the MDA-MB-231 cell line (**Fig 5I**).

## 1 Model selection

2 AIC values are calculated for each replicate culture for models 1, 2, and 3; the AIC allows  
3 comparison of the goodness of fit for models with varying numbers of free parameters. Across  
4 648 replicate cultures calibrated to models 1, 2, and 3, the AIC indicates that model 1 is optimal  
5 in 382 replicates (59.0%), model 2 is optimal in 129 replicates (19.9%), and model 3 is optimal in  
6 137 replicates (21.1%). This suggests that model 1 achieves the best overall performance across  
7 the range of conditions analyzed; however, models 2 and 3 are selected in a substantial minority  
8 of cases, and a more detailed investigation of the structure of these model preferences is available  
9 in the Supporting Information, structure of model preferences section (see **Fig S5** and **Fig S6**).  
10 Critical time projections and model validation results are constructed using model 1.

11

12



13

14 **Fig 6. Examples of model fitting demonstrate the ability of model 1 to capture long term**  
15 **dynamics.**

16 Examples of model fitting are shown for a single replicate culture in the MCF7 (A), BT474 (B),  
17 and MDA-MB-231 (C) cell lines. The curve represents a response to the doxorubicin  
18 concentration used in serial treatment within the cell line – 75 nM for the MCF7 line, 35 nM for  
19 the BT474 cell line, and 200 nM for the MDA-MB-231 cell line. Data is shown as open blue  
20 circles, while the best-fit curve for model 1 is shown in black, with the resistant and sensitive  
21 compartments shown in red and green respectively.

22

## 1 **Model validation**

2 A leave-one-out cross validation is used to test the predictive capability of model 1. Across  
3 143,093 total points evaluated, 80.6% fall within the 95% confidence interval. These results are  
4 summarized in **Table 3**, with a more detailed breakdown in **Table S4** in the supporting  
5 information.

6

<b>Condition</b>	<b>Points Evaluated</b>	<b>Within 95% CI</b>
Overall	143093	80.6%
All cell lines, recovering wells	94824	89.8%
All cell lines, dying wells	48269	62.5%
MCF7 cell line, total	42442	88.0%
MCF7 cell line, recovering wells	25992	94.5%
MCF7 cell line, dying wells	16450	77.7%
BT474 cell line, total	56923	75.1%
BT474 cell line, recovering wells	41391	87.3%
BT474 cell line, dying wells	15532	42.4%
MDA-MB-231 cell line, total	43728	80.7%
MDA-MB-231 cell line, recovering wells	27441	89.1%
MDA-MB-231 cell line, dying wells	16287	66.4%

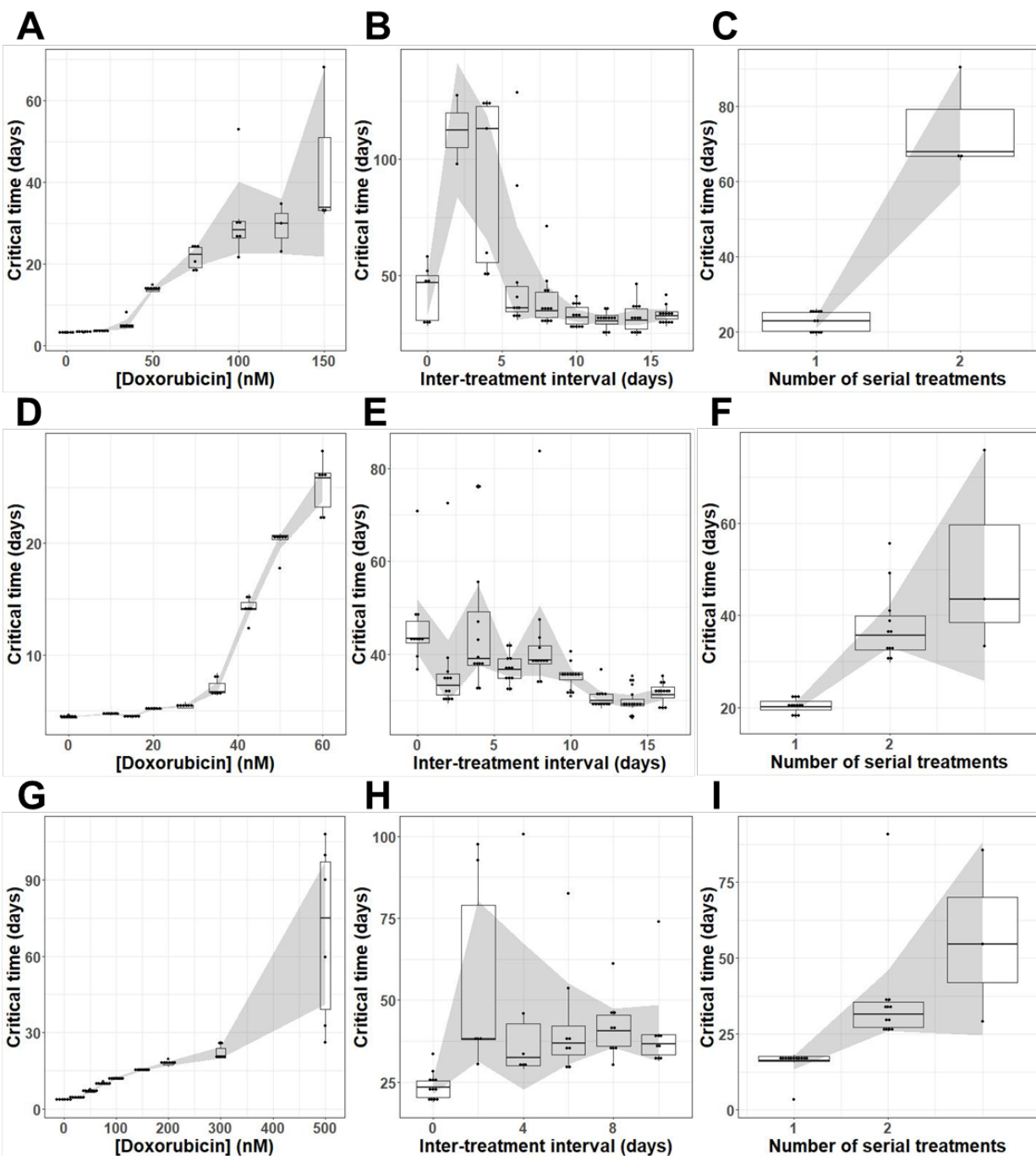
7 **Table 3. Leave-one-out cross validation.** The performance of model 1 at predicting data  
8 excluded from the training set is broken down by cell line and whether the replicate culture  
9 recovered or not (see Figure 4).

10

11 Model performance varies between cell lines and with recovery status. Model 1 performs best in  
12 the MCF7 cell line (88% of data in the 95% confidence interval), less well in the MDA-MB-231  
13 cell line (80.7% of data in the 95% confidence interval), and worst in the BT474 cell line (75.1%  
14 of data in the 95% confidence interval). Wells which recover are better modeled (89.8% of data  
15 within the 95% confidence interval) than wells which do not (62.5% of data within the 95%  
16 confidence interval). These results indicate that model 1 captures a significant portion (but not all)  
17 of the variation in the population level response to doxorubicin.

## 1 **Critical time projection**

2           After doxorubicin treatment, the cancer cell populations varied in rate of cell number  
3 decrease, lag time to net re-growth, and re-growth rate (**Fig 3**). Some cell populations remain  
4 quiescent and never initiate re-growth within the time of the experiment (**Fig 4**). To allow more  
5 precise and consistent comparison across the range of conditions explored in these experiments,  
6 we define a cell population as having recovered from the drug perturbation at the time, referred to  
7 as the critical time, when the population reaches twice the initial cell number for that replicate  
8 culture. This definition prioritizes the long term regrowth of a culture over its immediate response;  
9 for example, a culture which experiences a small decline in total population, but very slow  
10 regrowth, could be identified as having a longer recovery time than a culture which experiences a  
11 steep drop in population but very rapid regrowth. Utilizing a definition of cancer cell recovery or  
12 progression based on the initial population has been found to avoid counterintuitive results(55). It  
13 also enables comparison of cultures which do not experience a drop in total population, but which  
14 do vary in growth rate, such as those exposed to a low concentration of doxorubicin (**Fig 3A**). In  
15 some cultures, regrowth to twice the original cell number is not observed before the end of the  
16 experiment. To enable the inclusion of these results, we use model projections of the critical time  
17 based on the best-fit curve of the optimal model identified by model selection.



1  
2

### 3 Fig 7. Critical time projections.

4 Critical time is estimated based on the best fit to model 1 for each replicate culture in the MCF7  
5 cell lines and shown as a Tukey box-and-whiskers plot as doxorubicin concentration varies in the  
6 MCF7 cell line (A), the BT474 cell line (D), and the MDA-MB-231 cell line (G), as the interval  
7 between two 24 hour doxorubicin exposures varies at 75 nM in the MCF7 cell line (B), at 35 nM  
8 in the BT474 cell line (E), and at 200 nM in the MDA-MB-231 cell line (H), and as the number

1 of sequential 24 hour doxorubicin exposures varies at a two day interval and 75 nM in the MCF7  
2 cell line (C), at a zero day interval (continuous exposure) and 35 nM in the BT474 cell line (F),  
3 and at a two day interval and 200 nM in the MDA-MB-231 cell line (I). The number of  
4 replicates in each group varies between 3 and 12; all replicates in which recovery is observed are  
5 included. The 95% confidence interval on the mean is shown by the shaded region.  
6  
7

8 As the concentration of doxorubicin in a single exposure increases, the critical time  
9 increases in all three cell lines (**Fig 7A, 7D, 7G**). When the interval between two 75 nM  
10 doxorubicin exposures is varied in the MCF7 cell line (**Fig 7B**), and when the interval between  
11 two 200 nM doxorubicin exposures is varied in the MDA-MB-231 cell line (**Fig 7H**), a peak in  
12 the critical time is observed for both cell lines at a two day inter-treatment interval; this suggests  
13 that the cell population is sensitized to retreatment at this time. This result is consistent with the  
14 observation that 9/12 replicate cultures treated with this regimen in the MCF7 cell line and 6/12  
15 replicate cultures treated with this regimen in the MDA-MB-231 cell line never recover (**Fig 4B,**  
16 **4H**), and with the observation that the period of growth arrest is elevated at this time (**Fig 5B, 5H**).  
17 When the interval between two 35 nM doxorubicin exposures is varied in the BT474 cell line, the  
18 critical time is elevated at intervals of zero to eight days (**Fig 7E**), which is consistent with the  
19 elevated period of growth arrest observed in these replicates (**Fig 5E**). When the number of  
20 sequential treatments with 75 nM doxorubicin and a two day inter-treatment interval in the MCF7  
21 cell line is varied, the critical time increases on a second treatment (**Fig 7C**); the critical time for a  
22 third treatment cannot be obtained because no replicates treated with this regimen recovered (**Fig**  
23 **4C**). When the number of sequential treatments with 35 nM doxorubicin and no inter-treatment  
24 interval is varied in the BT474 cell line, the critical time increases for the second and third  
25 treatment (**Fig 7F**), and cannot be obtained for the fourth and fifth treatment because too few  
26 replicate wells recovered. Similarly, when the number of sequential treatments with 200 nM  
27 doxorubicin and a two day inter-treatment interval is varied in the MDA-MB-231 cell line, the  
28 critical time increases after a second and third treatment, and cannot be obtained for the fourth  
29 treatment because no replicates treated with that regimen recovered (**Fig 5I**).  
30



1  
2  
3  
4  
5  
6  
7  
8  
9  
10  
11  
12  
13  
14  
15  
16  
17  
18  
19  
20  
21  
22  
23  
24  
25  
26  
27  
28

## Methods

### Cell Culture

MCF7 (ATCC HTB-22) cells were cultured in Minimum Essential Media (MEM) (Gibco), supplemented with 10% fetal bovine serum (FBS) and 1% penicillin-streptomycin (P/S) (Gibco); these cells were maintained at 37° C in a 5% CO<sub>2</sub> atmosphere(56).

BT474 (ATCC HTB-20) cells were cultured in Richter’s Modification MEM (IMEM) (Corning), supplemented with 10% FBS, 1% P/S, and 20 µg/mL insulin; these cells were maintained at 37° C in a 5% CO<sub>2</sub> atmosphere(57).

MDA-MB-231 (ATCC HTB-26) cells were cultured in Dulbecco’s Modified Eagle Media (DMEM) (Gibco) supplemented with 5% FBS and 1% P/S; these cells were maintained at 37° C in a 5% CO<sub>2</sub> atmosphere(58).

To facilitate the use of fluorescent microscopy and automated cell quantification, stable fluorescent cell lines were established (MCF7-EGFPNLS1, BT474-GNS2, 231-GNS) expressing constitutive EGFP with a nuclear localization signal. Genomic integration of the EGFP expression cassette was accomplished utilizing the Sleeping Beauty transposon system. The EGFP-NLS sequence was obtained as a gBlock (IDT) and cloned into the optimized Sleeping Beauty transfer vector pSBbi-Neo. pSBbi-Neo was a gift from Eric Kowarz (Addgene plasmid #60525)(59). To mediate genomic integration, this two-plasmid system consisting of the transfer vector containing the EGFP-NLS sequence and the pCMV(CAT)T7-SB100 plasmid containing the Sleeping Beauty transposase was co-transfected into the MCF-7 population utilizing Lipofectamine 2000. mCMV(CAT)T7-SB100 was a gift from Zsuzsanna Izsvak (Addgene plasmid # 34879)(60). Following gene integration with Sleeping Beauty transposase, eGFP+ cells were collected by fluorescence activated cell sorting and maintained in media supplemented with 200 ng/mL G418 in place of P/S.

## 1 **Doxorubicin Treatment**

2 Doxorubicin hydrochloride (Cayman Chemical 15007) is reconstituted in water. Cell  
3 culture media is replaced with complete growth media containing doxorubicin at the specified  
4 concentration. After 24 hours, doxorubicin media is replaced with drug-free media.

## 5 **Long term doxorubicin response experiments**

6 Cells are seeded in a 96-well plate at target densities of 2,000 cells per well. Fluorescent  
7 and phase contrast images are collected at intervals of 4 hours or shorter throughout the study in  
8 the Incucyte S2 Live Cell Analysis System (Essen/Sartorius) with temperature and environmental  
9 control. Cells are initially seeded in 100  $\mu$ L growth media per well and cultured for 2 days to  
10 allow cell adhesion and recovery from the passaging process. Drug treatment is performed by  
11 adding 100  $\mu$ L growth media containing doxorubicin at 2x the desired final concentration, with 6  
12 or 12 replicates for each experimental condition. After 24 hours, the drug exposure is ended by  
13 aspirating the media, and replacing with fresh growth media. Images collection is continued for  
14 21-56 days at a frequency between once per two hours and once per four hours; the duration of  
15 image collection is selected such that all wells in which any cells recover proliferation are allowed  
16 to reach the logistic growth stage.

## 17 **Image Analysis**

18 Cell counting is performed using the green fluorescence channel using standard image  
19 analysis techniques: background subtraction, followed by thresholding, edge detection, and a  
20 minimum area filter. These settings have been optimized for accuracy and robustness in handling  
21 the image-to-image variation in acquired images.

## 22 **Data normalization**

23 The data for each replicate culture is truncated to ensure that only accurate, meaningful  
24 data is used for model calibration. Time course cell number data for each replicate culture is  
25 truncated at 30,000 cells or when the counted cell number drops by more than 50% as a result of

1 media handling, or when the cell count becomes unreliable as indicated by repeated discontinuities  
2 in the cell number vector. In the case of a single discontinuity where fewer than half of the cells  
3 are lost, the data is instead normalized to remove the discontinuity; this normalization is performed  
4 by specifying that the cell number for time points prior to the discontinuity will be divided by a  
5 constant  $\alpha$ , calculated such that the first and second derivative of the cell number are smooth across  
6 the discontinuity:

$$7 \quad \alpha = \frac{\frac{(N_{d-1} - N_{d-2})}{(t_{d-1} - t_{d-2})} + 2 \frac{N_{d-1}}{t_d - t_{d-1}}}{2 \frac{N_d}{t_d - t_{d-1}} + \frac{N_d - N_{d+1}}{t_{d+1} - t_d}}$$

8 Here  $N_d$  is the cell number just after the discontinuity,  $N_{d-1}$  is the cell number just before  
9 the discontinuity, and so on.

## 10 **Quantification of $t_r$**

11 To find the proliferation delay,  $t_r$ , a density-based clustering technique (DBSCAN) was  
12 used to find an initial clustering of cells after treatment had been applied. The optimal parameters  
13 for DBSCAN were manually calibrated for each plate. Once a sufficiently large cluster of cells  
14 was properly identified, the cluster was tracked backwards in time. At each previous timepoint,  
15 DBSCAN was again used to identify the location of the cluster. When a timepoint was identified  
16 at which clustering could no longer be found, the proliferation delay was determined as the  
17 difference in hours between that timepoint and the time of initial treatment.

## 18 **Model calibration**

19 Model parameters are extracted from time course cell population data by calibrating the  
20 three models to the cell number vector for each replicate culture using a nonlinear least-squares  
21 approach implemented in MATLAB.

22

## 23 **Data Availability**

1 All cell number data in this manuscript, as well as all MATLAB scripts used for model  
2 calibration and validation, are available at [https://github.com/brocklab/Drug-Response-Dynamics-](https://github.com/brocklab/Drug-Response-Dynamics-Model-Calibration)  
3 Model-Calibration.

## 4 5 **Discussion**

6 The use of longitudinal monitoring *via* time-lapse microscopy allowed us to implement  
7 and compare dynamic models of drug sensitivity. This allowed us to identify conditions in which  
8 a model incorporating a delay on sensitive cell death is preferred over the more common, simpler  
9 model, and to determine that across the range of conditions tested, a model describing that delay  
10 with an exponential time constant performs best. Additionally, our model selection work identified  
11 the parameters  $f_r$  and  $t_r$  as computationally non-separable. Quantification of  $t_r$  *via* automated  
12 clustering analysis confirmed the existence of a delay in proliferation under some conditions.  
13 Incorporating these two time delays removed sources of systematic error and allowed extraction  
14 of more accurate values for key model parameters such as the resistant fraction and post-recovery  
15 growth rate via calibration.

16 We identified transient changes in doxorubicin sensitivity following an initial doxorubicin  
17 exposure. Inter-treatment interval proved to be an optimizable factor in drug scheduling, with  
18 retreatment during the window of transient sensitivity increasing the total time to population  
19 doubling by 104% in the MCF7 line, 46% in the BT474 line, and 40% in the MDA-MB-231 line,  
20 compared to treatment with an identical total amount of drug with an interval such that drug  
21 sensitivity had stabilized. In addition to extending the time to population doubling, treatment at  
22 the optimal time actually resulted in elimination of the cancer cell population in 9/12 replicate  
23 cultures in the MCF7 cell line and 6/12 replicate cultures in the MDA-MB-231 cell line. The  
24 optima identified for these cell lines did not depend on any single model parameter; they result  
25 from the interaction of all three relevant parameters, each of which changes dynamically with a  
26 different characteristic time.

1           Although this mathematical modeling-based approach enabled the identification of key  
2 features of the dynamic response which have previously not been recognized (i.e., the time delays  
3 on both death and proliferation) it does have limitations. While model 1 was selected over the  
4 existing bi-exponential model in all three cell lines, the improvement in performance varied with  
5 cell line. The calibrated model allowed identification of optimal retreatment intervals in the MCF7  
6 and MDA-MB-231 cell lines, but did not offer a clear equivalent in the BT474 cell line. This is  
7 likely due to differences in drug sensitivity and timing of response that characterize each cell line  
8 –BT474 has higher sensitivity and responds more slowly; consequently it was treated at a lower  
9 dose range. It is likely that the optimal model to describe growth dynamics varies with cell line,  
10 and possible that the most relevant mechanisms of changing drug sensitivity vary with cell line.  
11 A second significant limitation of this approach is that it is phenomenological, and neither relies  
12 on nor contributes to understanding of the underlying mechanisms.

13           The approach described here allows for high throughput, high time resolution measurement  
14 of population-averaged properties. In particular, multidrug treatment would greatly benefit from  
15 longitudinal monitoring of population dynamics. Collateral sensitivity, a phenomenon where one  
16 drug causes a cell population to become sensitive to a second drug(61), has shown increasing  
17 promise *in-vitro*(62,63). Notably, Dhawan et al. found that specific intervals between drugs was  
18 necessary in order to identify pairs of collaterally sensitive drugs. Furthermore, the repeatability  
19 of collateral sensitivity to drug-resistant populations has yet to be fully understood(64,65). Thus,  
20 being able to perform high throughput measurement would allow for pairs of collaterally sensitive  
21 drugs to not only be found but evaluated as potential treatments. Additionally, the approach  
22 demonstrated here would allow for optimal control theory to be experimentally evaluated, a  
23 strategy which can be used to find optimal treatment strategies for a dynamical system(66).  
24 Optimal control theory requires a detailed and accurate understanding of the relationship between  
25 controllable variables such as drug concentration and inter-treatment interval and biological  
26 variables such as the resistant fraction and post-treatment regrowth rate. The experimental and  
27 computational methods described here allow for the development of such detailed data sets.

1 Optimal control theory has recently been used to find optimal scheduling(67,68), but has yet to be  
2 evaluated in an *in-vitro* setting. The development of drug response models with sufficient detail  
3 for use in predicting collateral sensitivity and testing optimal control theory could additionally  
4 contribute to the field of adaptive therapy, in which treatment is modified based on feedback  
5 regarding a patient's individual response(69). This approach currently shows significant promise  
6 in the treatment of prostate cancer(70), and the development of more detailed drug response  
7 models can contribute to the extension of these techniques to additional cancer types. Single cell  
8 sequencing technologies promise to provide great insight into the mechanistic underpinnings of  
9 this heterogeneity in drug sensitivity(65,71); however, throughput for these technologies remains  
10 low enough (and expense remains high enough) that directly assessing dynamic changes in drug  
11 sensitivity over short time scales remains difficult.

12         These two approaches can complement each other, with longitudinal studies such as the  
13 ones described here identifying key time scales and single cell transcriptomic studies enhancing  
14 mechanistic insight. This suggests several potentially productive avenues for continuing work:  
15 Additional longitudinal studies can extend the techniques demonstrated here to new drugs, new  
16 cell lines and new cancer types. Along with the development of new data sets, exploration of  
17 additional cancer growth models will allow deeper understanding of what features of a cell line  
18 (drug sensitivity, growth rate, clonal heterogeneity, etc.) correspond to particular optimal growth  
19 models. The data presented here also indicate time points that would be of particular interest for  
20 future single-cell studies, such as the two day post treatment optimal treatment interval in the  
21 MCF7 and MDA-MB-231 cell lines. Such studies could elucidate the mechanisms underlying  
22 these early changes in drug sensitivity, and could in turn enable another generation of longitudinal  
23 studies in cell lines engineered with fluorescent reporters coupled to mechanisms thus identified.

24         Finally, while these methods are several steps removed from clinically actionable at this  
25 point, there is potential to contribute to preclinical drug development. *In vitro* mechanistic studies  
26 and preclinical screening often report cell death at a single end point 24-72 hours after treatment;  
27 this is insufficient to quantify the long-term drug response of the cell population. Longitudinal

1 studies such as these, implemented iteratively to identify key time scales such as the optimal inter-  
2 treatment interval, could allow further optimization of drug treatment schedules to inform  
3 preclinical testing.

#### 4 5 **Conclusions**

6 Using an integrated experimental-computational approach, we identified a biexponential  
7 model of drug response including time dependence in post-treatment proliferation and death rates  
8 as superior to a static (time independent) model. The delay of proliferation in drug resistant cells  
9 is a key variable, and was computationally non-separable from the resistant fraction; consequently,  
10 measurement of the proliferation delay is a necessary prerequisite to accurate model calibration.  
11 The inter-treatment interval of a multi-dose series was found to be an optimizable parameter of the  
12 treatment schedule, increasing the time to a proliferation metric by 40%-106% in three breast  
13 cancer cell lines.

#### 14 15 **Acknowledgements**

16 We would like to thank Yasmeen K. Zubair and Isha Patel for their work in data collection and  
17 processing during the preliminary experiments which initiated this work. We are grateful for  
18 funding through the NIH via R01CA226258 and U01CA253540 to A.B. and NCI U01 CA142565,  
19 NCI U01 CA174706, NCI U24 CA226110, NCIR01CA240589, and CPRIT RR160005. To T.E.Y.  
20 T.E.Y. is a CPRIT Scholar of Cancer Research. The authors declare no conflicts of interest.

#### 21 22 **Data sharing**

23 All cell number data in this manuscript, as well as all MATLAB scripts used for model calibration  
24 and validation, are available at [https://github.com/brocklab/Drug-Response-Dynamics-Model-  
25 Calibration](https://github.com/brocklab/Drug-Response-Dynamics-Model-Calibration).

26  
27

## References

1. Heron M. Deaths: Leading Causes for 2017. *Natl Vital Stat Rep*. 2019 Jun 24;68(6).
2. Longley DB, Johnston PG. Molecular mechanisms of drug resistance. *J Pathol*. 2005 Jan;205(2):275–92.
3. McKenna MT, Weis JA, Brock A, Quaranta V, Yankeelov TE. Precision Medicine with Imprecise Therapy: Computational Modeling for Chemotherapy in Breast Cancer. *Transl Oncol*. 2018 Jun;11(3):732–42.
4. Jarrett AM, Lima EABF, Hormuth DA, McKenna MT, Feng X, Ekrut DA, et al. Mathematical Models of Tumor Cell Proliferation: A Review of the Literature. *Expert Rev Anticancer Ther*. 2018 Dec;18(12):1271–86.
5. Altrock PM, Liu LL, Michor F. The mathematics of cancer: integrating quantitative models. *Nat Rev Cancer*. 2015 Dec;15(12):730–45.
6. Moreno L, Pearson AD. How can attrition rates be reduced in cancer drug discovery? *Expert Opin Drug Discov*. 2013 Apr 1;8(4):363–8.
7. Le Tourneau C, Lee JJ, Siu LL. Dose Escalation Methods in Phase I Cancer Clinical Trials. *JNCI J Natl Cancer Inst*. 2009 May 20;101(10):708–20.
8. Gottlieb JA, Rivkin SE, Spigel SC, Hoogstraten B, O'Bryan RM, Delaney FC, et al. Superiority of adriamycin over oral nitrosoureas in patients with advanced breast carcinoma. A southwest cancer chemotherapy study group study. *Cancer*. 1974;33(2):519–26.
9. Brock A, Chang H, Huang S. Non-genetic heterogeneity--a mutation-independent driving force for the somatic evolution of tumours. *Nat Rev Genet*. 2009 May;10(5):336–42.
10. Turashvili G, Brogi E. Tumor Heterogeneity in Breast Cancer. *Front Med*. 2017;4:227.
11. Abramson VG, Mayer IA. Molecular Heterogeneity of Triple Negative Breast Cancer. *Curr Breast Cancer Rep*. 2014 Sep 1;6(3):154–8.
12. Pi B, Ar H, Mj R, Li S. Tumour heterogeneity in the clinic. *Nature*. 2013;501(7467):355–64.
13. Burrell R, Mcgranahan N, Bartek J, Swanton C. The Causes and Consequences of Genetic Heterogeneity in Cancer Evolution. *Nature*. 2013 Sep 19;501:338–45.
14. Wolman SR, Heppner GH. Genetic heterogeneity in breast cancer. *J Natl Cancer Inst*. 1992 Apr 1;84(7):469–70.
15. Brooks MD, Burness ML, Wicha MS. Therapeutic Implications of Cellular Heterogeneity and Plasticity in Breast Cancer. *Cell Stem Cell*. 2015 Sep 3;17(3):260–71.



16. Håkansson L, Tropé C. On the Presence Within Tumours of Clones That Differ in Sensitivity to Cytostatic Drugs. *Acta Pathol Microbiol Scand [A]*. 1974;82A(1):35–40.
17. Davila E, Amazon K. The Clinical Importance of the Heterogeneity of HER2 neu. *Case Rep Oncol*. 2010;3(2):268–71.
18. McGranahan N, Swanton C. Biological and Therapeutic Impact of Intratumor Heterogeneity in Cancer Evolution. *Cancer Cell*. 2015 Jan 12;27(1):15–26.
19. Norton L, Simon R. Tumor size, sensitivity to therapy, and design of treatment schedules. *Cancer Treat Rep*. 1977 Oct;61(7):1307–17.
20. Norton L, Simon R. Growth Curve of an Experimental Solid Tumor Following Radiotherapy. *J Natl Cancer Inst*. 1977 Jul 1;58:1735–41.
21. Norton L, Simon R. The Norton-Simon hypothesis revisited. *Cancer Treat Rep*. 1986 Jan;70(1):163–9.
22. Bonadonna G, Zambetti M, Valagussa P. Sequential or alternating doxorubicin and CMF regimens in breast cancer with more than three positive nodes. Ten-year results. *JAMA*. 1995 Feb 15;273(7):542–7.
23. Bonadonna G, Zambetti M, Moliterni A, Gianni L, Valagussa P. Clinical relevance of different sequencing of doxorubicin and cyclophosphamide, methotrexate, and Fluorouracil in operable breast cancer. *J Clin Oncol Off J Am Soc Clin Oncol*. 2004 May 1;22(9):1614–20.
24. Citron ML, Berry DA, Cirincione C, Hudis C, Winer EP, Gradishar WJ, et al. Randomized trial of dose-dense versus conventionally scheduled and sequential versus concurrent combination chemotherapy as postoperative adjuvant treatment of node-positive primary breast cancer: first report of Intergroup Trial C9741/Cancer and Leukemia Group B Trial 9741. *J Clin Oncol Off J Am Soc Clin Oncol*. 2003 Apr 15;21(8):1431–9.
25. Liu Y, Gu F, Liang J, Dai X, Wan C, Hong X, et al. The efficacy and toxicity profile of metronomic chemotherapy for metastatic breast cancer: A meta-analysis. *PloS One*. 2017;12(3):e0173693.
26. Munzone E, Colleoni M. Clinical overview of metronomic chemotherapy in breast cancer. *Nat Rev Clin Oncol*. 2015 Nov;12(11):631–44.
27. Hanahan D, Bergers G, Bergsland E. Less is more, regularly: metronomic dosing of cytotoxic drugs can target tumor angiogenesis in mice. *J Clin Invest*. 2000 Apr;105(8):1045–7.
28. Kaur H, Budd GT. Metronomic therapy for breast cancer. *Curr Oncol Rep*. 2004 Jan;6(1):49–52.

29. Munoz R, Shaked Y, Bertolini F, Emmenegger U, Man S, Kerbel RS. Anti-angiogenic treatment of breast cancer using metronomic low-dose chemotherapy. *Breast Edinb Scotl*. 2005 Dec;14(6):466–79.
30. Almeida L, Bagnerini P, Fabrini G, Hughes BD, Lorenzi T. Evolution of cancer cell populations under cytotoxic therapy and treatment optimisation: insight from a phenotype-structured model. *ESAIM Math Model Numer Anal*. 2019 Jul;53(4):1157–90.
31. Greene JM, Sanchez-Tapia C, Sontag ED. Mathematical Details on a Cancer Resistance Model. *Front Bioeng Biotechnol* [Internet]. 2020 Jun 17 [cited 2021 Jan 22];8. Available from: <https://www.ncbi.nlm.nih.gov/pmc/articles/PMC7325889/>
32. Olivier A, Pouchol C. Combination of Direct Methods and Homotopy in Numerical Optimal Control: Application to the Optimization of Chemotherapy in Cancer. *J Optim Theory Appl*. 2019 May 1;181(2):479–503.
33. Pouchol C, Clairambault J, Lorz A, Trélat E. Asymptotic analysis and optimal control of an integro-differential system modelling healthy and cancer cells exposed to chemotherapy. *J Mathématiques Pures Appliquées*. 2016 Dec 14;
34. AbuHammad S, Zihlif M. Gene expression alterations in doxorubicin resistant MCF7 breast cancer cell line. *Genomics*. 2013 Apr;101(4):213–20.
35. Gottesman MM. Mechanisms of cancer drug resistance. *Annu Rev Med*. 2002;53:615–27.
36. Hill RP, Chambers AF, Ling V, Harris JF. Dynamic heterogeneity: rapid generation of metastatic variants in mouse B16 melanoma cells. *Science*. 1984 Jun 1;224(4652):998–1001.
37. Kuukasjärvi T, Karhu R, Tanner M, Kähkönen M, Schäffer A, Nupponen N, et al. Genetic heterogeneity and clonal evolution underlying development of asynchronous metastasis in human breast cancer. *Cancer Res*. 1997 Apr 15;57(8):1597–604.
38. Simpson PT, Reis-Filho JS, Gale T, Lakhani SR. Molecular evolution of breast cancer. *J Pathol*. 2005 Jan;205(2):248–54.
39. Balko JM, Giltnane JM, Wang K, Schwarz LJ, Young CD, Cook RS, et al. Molecular profiling of the residual disease of triple-negative breast cancers after neoadjuvant chemotherapy identifies actionable therapeutic targets. *Cancer Discov*. 2014 Feb;4(2):232–45.
40. Duncan JS, Whittle MC, Nakamura K, Abell AN, Midland AA, Zawistowski JS, et al. Dynamic reprogramming of the kinome in response to targeted MEK inhibition in triple-negative breast cancer. *Cell*. 2012 Apr 13;149(2):307–21.
41. Navin N, Krasnitz A, Rodgers L, Cook K, Meth J, Kendall J, et al. Inferring tumor progression from genomic heterogeneity. *Genome Res*. 2010 Jan;20(1):68–80.

42. Levsky JM, Shenoy SM, Pezo RC, Singer RH. Single-cell gene expression profiling. *Science*. 2002 Aug 2;297(5582):836–40.
43. Dalerba P, Kalisky T, Sahoo D, Rajendran PS, Rothenberg ME, Leyrat AA, et al. Single-cell dissection of transcriptional heterogeneity in human colon tumors. *Nat Biotechnol*. 2011 Dec;29(12):1120–7.
44. Jolly MK, Kulkarni P, Weninger K, Orban J, Levine H. Phenotypic Plasticity, Bet-Hedging, and Androgen Independence in Prostate Cancer: Role of Non-Genetic Heterogeneity. *Front Oncol* [Internet]. 2018 [cited 2021 Jan 22];8. Available from: <https://www.frontiersin.org/articles/10.3389/fonc.2018.00050/full>
45. Singh DK, Ku C-J, Wichaidit C, Steininger RJ, Wu LF, Altschuler SJ. Patterns of basal signaling heterogeneity can distinguish cellular populations with different drug sensitivities. *Mol Syst Biol*. 2010 May 11;6:369.
46. Sigal A, Milo R, Cohen A, Geva-Zatorsky N, Klein Y, Liron Y, et al. Variability and memory of protein levels in human cells. *Nature*. 2006 Nov;444(7119):643–6.
47. Pisco AO, Brock A, Zhou J, Moor A, Mojtahedi M, Jackson D, et al. Non-Darwinian dynamics in therapy-induced cancer drug resistance. *Nat Commun*. 2013 Dec;4(1):2467.
48. Pisco AO, Huang S. Non-genetic cancer cell plasticity and therapy-induced stemness in tumour relapse: “What does not kill me strengthens me.” *Br J Cancer*. 2015 May 26;112(11):1725–32.
49. Sharma SV, Lee DY, Li B, Quinlan MP, Takahashi F, Maheswaran S, et al. A chromatin-mediated reversible drug-tolerant state in cancer cell subpopulations. *Cell*. 2010 Apr 2;141(1):69–80.
50. Flusberg DA, Roux J, Spencer SL, Sorger PK. Cells surviving fractional killing by TRAIL exhibit transient but sustainable resistance and inflammatory phenotypes. *Mol Biol Cell*. 2013 Jul;24(14):2186–200.
51. Chatterjee MS, Elassaiss-Schaap J, Lindauer A, Turner DC, Sostelly A, Freshwater T, et al. Population Pharmacokinetic/Pharmacodynamic Modeling of Tumor Size Dynamics in Pembrolizumab-Treated Advanced Melanoma. *CPT Pharmacomet Syst Pharmacol*. 2017 Jan;6(1):29–39.
52. Hokanson JA, Brown BW, Thompson JR, Drewinko B, Alexanian R. Tumor growth patterns in multiple myeloma. *Cancer*. 1977 Mar;39(3):1077–84.
53. K. W, et al. Precision medicine by modeling pharmacokinetic and biomarker drivers of tumor kinetics: assessing effects of alsertib exposure and target SNP status on antitumor activity. *CPT Pharmacomet Syst Pharmacol*. 2017;101(S1):S5–99.

54. McKenna MT, Weis JA, Barnes SL, Tyson DR, Miga MI, Quaranta V, et al. A Predictive Mathematical Modeling Approach for the Study of Doxorubicin Treatment in Triple Negative Breast Cancer. *Sci Rep*. 2017 Jul 18;7(1):5725.
55. Johnson K, Gomez A, Burton J, White D, Chakravarty A, Schmid A, et al. Directional inconsistency between Response Evaluation Criteria in Solid Tumors (RECIST) time to progression and response speed and depth. *Eur J Cancer*. 2019 Mar 1;109:196–203.
56. Soule HD, Vazquez J, Long A, Albert S, Brennan M. A human cell line from a pleural effusion derived from a breast carcinoma. *J Natl Cancer Inst*. 1973 Nov;51(5):1409–16.
57. Lasfargues EY, Coutinho WG, Redfield ES. Isolation of two human tumor epithelial cell lines from solid breast carcinomas. *J Natl Cancer Inst*. 1978 Oct;61(4):967–78.
58. Cailleau R, Olivé M, Cruciger QV. Long-term human breast carcinoma cell lines of metastatic origin: preliminary characterization. *In Vitro*. 1978 Nov;14(11):911–5.
59. Kowarz E, Löscher D, Marschalek R. Optimized Sleeping Beauty transposons rapidly generate stable transgenic cell lines. *Biotechnol J*. 2015 Apr;10(4):647–53.
60. Mátés L, Chuah MKL, Belay E, Jerchow B, Manoj N, Acosta-Sanchez A, et al. Molecular evolution of a novel hyperactive Sleeping Beauty transposase enables robust stable gene transfer in vertebrates. *Nat Genet*. 2009 Jun;41(6):753–61.
61. Pluchino KM, Hall MD, Goldsborough AS, Callaghan R, Gottesman MM. Collateral sensitivity as a strategy against cancer multidrug resistance. *Drug Resist Updat*. 2012 Feb;15(1–2):98–105.
62. Dhawan A, Nichol D, Kinose F, Abazeed ME, Marusyk A, Haura EB, et al. Collateral sensitivity networks reveal evolutionary instability and novel treatment strategies in ALK mutated non-small cell lung cancer. *Sci Rep*. 2017 Dec;7(1):1232.
63. Acar A, Nichol D, Fernandez-Mateos J, Cresswell GD, Barozzi I, Hong SP, et al. Exploiting evolutionary steering to induce collateral drug sensitivity in cancer. *Nat Commun*. 2020 Apr 21;11(1):1–14.
64. Nichol D, Rutter J, Bryant C, Hujer AM, Lek S, Adams MD, et al. Antibiotic collateral sensitivity is contingent on the repeatability of evolution. *Nat Commun*. 2019 Dec;10(1):334.
65. Scarborough JA, McClure E, Anderson P, Dhawan A, Durmaz A, Lessnick SL, et al. Identifying States of Collateral Sensitivity during the Evolution of Therapeutic Resistance in Ewing’s Sarcoma. *iScience*. 2020 Jul 24;23(7):101293.
66. Jarrett AM, Faghihi D, Ii DAH, Lima EABF, Virostko J, Biros G, et al. Optimal Control Theory for Personalized Therapeutic Regimens in Oncology: Background, History, Challenges, and Opportunities. *J Clin Med*. 2020 May 2;9(5):1314.

67. Yoon N, Vander Velde R, Marusyk A, Scott JG. Optimal Therapy Scheduling Based on a Pair of Collaterally Sensitive Drugs. *Bull Math Biol.* 2018 Jul 1;80(7):1776–809.
68. Gluzman M, Scott JG, Vladimirovsky A. Optimizing adaptive cancer therapy: dynamic programming and evolutionary game theory. :10.
69. Gatenby RA, Silva AS, Gillies RJ, Frieden BR. Adaptive Therapy. *Cancer Res.* 2009 Jun 1;69(11):4894–903.
70. Brady-Nicholls R, Nagy JD, Gerke TA, Zhang T, Wang AZ, Zhang J, et al. Prostate-specific antigen dynamics predict individual responses to intermittent androgen deprivation. *Nat Commun.* 2020 Apr 9;11(1):1750.
71. Kim C, Gao R, Sei E, Brandt R, Hartman J, Hatschek T, et al. Chemoresistance Evolution in Triple-Negative Breast Cancer Delineated by Single-Cell Sequencing. *Cell.* 2018 May;173(4):879-893.e13.